Solar Energy Materials and Solar Cells 174 (2018) 77–83

Contents lists available at ScienceDirect

Solar Energy Materials and Solar Cells

journal homepage: www.elsevier.com/locate/solmat

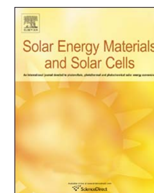

Electrical characterization and comparison of CIGS solar cells made with different structures and fabrication techniques

Rebekah L. Garris, Steve Johnston, Jian V. Li, Harvey L. Guthrey, Kannan Ramanathan, Lorelle M. Mansfield*

National Renewable Energy Laboratory, 15013 Denver West Parkway, Golden, CO 80401, USA

ARTICLE INFO

Keywords:
Admittance spectroscopy
Cross-sectional electron-beam induced current (EBIC)
$Cu(In,Ga)Se_2$ (CIGS)
Deep-level transient spectroscopy (DLTS)
Thin-film photovoltaics
Time-resolved photoluminescence (TRPL)

ABSTRACT

In a previous paper [1], we reported on $Cu(In,Ga)Se_2$-based (CIGS) solar cell samples collected from different research laboratories and industrial companies with the purpose of understanding the range of CIGS materials that can lead to high-quality and high-efficiency solar panels. Here, we report on electrical measurements of those same samples. Electron-beam induced current and time-resolved photoluminescence (TRPL) gave insights about the collection probability and the lifetime of carriers generated in each absorber. Capacitance and drive-level capacitance profiling revealed nonuniformity in carrier-density profiles. Admittance spectroscopy revealed small activation energies ($\leq$ 0.03 eV) indicative of the inversion strength, larger activation energies ($>$ 0.1 eV) reflective of thermal activation of absorber conductivity and a deeper defect level. Deep-level transient spectroscopy (DLTS) probed deep hole-trapping defects and showed that all samples in this study had a majority-carrier defect with activation energy between 0.3 eV and 0.9 eV. Optical-DLTS revealed deep electron-trapping defects in several of the CIGS samples. This work focused on revealing similarities and differences between high-quality CIGS solar cells made with various structures and fabrication techniques.

1. Introduction

Copper indium gallium diselenide (CIGS) is the basis for some of the most efficient thin-film solar cells available. The theoretical efficiency limit for CIGS is 29% [2], whereas the current world-record CIGS cell efficiency is 22.6% [3], and most CIGS module products have efficiencies in the 13–15% efficiency range. To address the cell-to-module gap in CIGS, the U.S. Department of Energy (DOE) and the National Science Foundation sponsored the Foundational Program to Advance Cell Efficiency (F-PACE). Our F-PACE team consists of the National Renewable Energy Laboratory (NREL), universities, and industrial partners. We address the DOE's SunShot Initiative module cost goal of $0.50 per watt by 2020 by investigating CIGS topics of broad interest and disseminating information to the scientific community. Under the F-PACE program, we partner with CIGS companies to solve process-specific problems so that they can increase the efficiency of their products.

In a previous study [1], we reported on high-quality CIGS solar cells fabricated at six laboratories from the F-PACE team; those cells were made with different compositions, structures, and deposition techniques. We measured significant variations in the bandgaps, bandgap profiles, carrier densities, and morphologies, but the device performance of the cells was similar. We investigated cell uniformity, internal quantum efficiencies, ideal diode parameters, parasitic resistances, voltage losses, and fill-factor losses. Through this investigation, we compared different device structures and absorber processes to approach tangible solutions for closing efficiency gaps between lab cells and large-scale manufacturing. This new report expands on our previous work, looking specifically at the underlying electrical behavior governing the performance of these CIGS-based solar cells made with different structures and fabrication processes.

2. Experimental

Solar cell samples were collected from six different fabricators consisting of research laboratories and industrial partners. Note that this is the same set of samples studied in our previous report, and that each sample contains 4–7 small-area devices. The selected samples represent an average device performance that would be expected from each fabrication process (described previously [1] and summarized in Table 1). Even though absorbers are a collection of $Cu(In,Ga)Se_2$ (CIGS), $(Ag,Cu)(In,Ga)Se_2$ (ACIGS), and $Cu(In,Ga)(S,Se)_2$ (CIGSSe), samples will all be referred to as CIGS. Performance parameters extracted from current density versus voltage (JV) are summarized in

* Corresponding author.
E-mail address: Lorelle.mansfield@nrel.gov (L.M. Mansfield).

http://dx.doi.org/10.1016/j.solmat.2017.08.027
Received 12 May 2017; Received in revised form 15 August 2017; Accepted 20 August 2017
Available online 31 August 2017
0927-0248/ Published by Elsevier B.V.

Table 1
Summary of cell structures and fabrication processes for six different fabricators, reprinted from [1].

Fabricator	Substrate	Absorber process	Absorber	Buffer	Cell structure
A	Glass	Three-stage Co-evaporation	$Cu(In,Ga)Se_2$	CdS	ZnO:Al/i-ZnO/CdS/CIGS/Mo
B	Glass	Three-stage Co-evaporation	$(Ag,Cu)(In,Ga)Se_2$	CdS	ITO[a]/i-ZnO/CdS/ACIGS/Mo
C	Stainless steel (R2R[b])	Co-sputtering	$Cu(In,Ga)Se_2$	CdS	ZnO:Al/i-ZnO/CdS/CIGS/Mo
D	Stainless steel (R2R)	Three-stage Co-evaporation	$Cu(In,Ga)Se_2$	CdS	ITO/i-ZnO/CdS/CIGS/Mo
E	Glass	Metal-precursor reaction with H_2Se/H_2S	$Cu(In,Ga)(S,Se,S,See)_2$	Thin CdS	ZnO:B/ZnO/CdS/CIGSSe/Mo
F	Glass	Metal-precursor reaction with H_2Se/H_2S	$Cu(In,Ga)(S,Se,S,See)_2$	Thin Zn(O,O,S)	ZnO:B/ZnO/Zn(O,O,S)/CIGSSe/Mo

[a] ITO is indium tin oxide.
[b] R2R is roll-to-roll.

Table 2
Parameter table from J-V curves of representative devices, reprinted from [1].

Sample	V_{OC} (mV)	J_{SC} (mA/cm^2)	*FF* (%)	η (%)	E_g (eV)
A	701	34.3	80.7	19.4	1.17
B	742	33.0	77.8	19.1	1.22
C	698	32.3	77.4	17.5	1.22
D	656	34.3	69.3	15.6	1.18
E	571	34.6	72.3	14.3	1.09
F	669	38.3	73.2	18.8	1.05

Table 2 [1]. Samples from each of the six fabricators will be identified herein by the letters A − F in this study, as indicated in Table 1.

Measurements were made on all six samples to compare electrical performance. Electron-beam induced current (EBIC) and time-resolved photoluminescence (TRPL) were measured to identify the location and the lifetime of carriers generated in each absorber. Capacitance versus voltage (CV), drive-level capacitance profiling (DLCP), admittance spectroscopy (AS), and deep-level transient spectroscopy (DLTS) were used to understand carrier densities and trap activation energies affecting carrier transport and recombination.

3. Results and discussion

3.1. Cross-sectional electron beam-induced current

EBIC measurements were performed in a field emission scanning electron microscope (FESEM) at 295 K, operated with a 5-kV accelerating voltage and a 1-nA beam current. Samples were prepared by cleaving films on glass substrates or cutting films on metal foils to expose the films for cross-sectional imaging. Sample D needed to be polished using 4-kV Ar+ ions to obtain an appropriate region for EBIC analysis. Fig. 1 shows overlaid images of EBIC and FESEM along with the EBIC intensity profile (white line) for each film, where the cross-sectional images are 8 µm wide and 5 µm vertical. The EBIC signal over the entire width of each image was averaged to produce the intensity profile for that film. However, due to the topography of the surface, the profile for sample F was created only over a smaller region of the film; the dashed line in the image indicates this area.

In comparing the images of samples on glass substrates (samples A, B, E, and F), the difference in morphology of the samples with CIGS absorbers deposited using metal precursors reacted with H_2Se/H_2S (2-step) and the samples made by three-stage co-evaporation (3-stage) are apparent. Samples A and B, made with a 3-stage process, had larger grains, whereas samples E and F, made with a 2-step process, had smaller grains. Samples A, E, and F show similar EBIC intensity profiles, with higher collection at the front of the device and lower collection toward the back. Sample B had more uniform collection throughout the film thickness, which could be due to the lower doping level in that absorber.

The samples that were grown on stainless steel (samples C and D) presented more of a challenge to prepare cross-sectional samples. Sample D was rather difficult to prepare because it delaminated when cut; it was polished to get a good cross-section, which is why the grain boundaries appear less defined in that image. Sample C was easier to prepare than sample D, but it also broke away from the substrate. Between these two, sample D had more uniform collection throughout the film thickness, and sample C exhibited more nonuniform collection both laterally and vertically through the film. Past analyses have shown that the Ar+ ion milling can affect the sharpness of particular features but the overall trends remain. Obviously the different growth processes and composition variations do change the electric field distribution. Although the connection between device properties and EBIC images is not clear, these images do give an interesting insight into the current collection probability in the cells.

3.2. Time-resolved photoluminescence

Minority-carrier (electron) lifetime is an important characteristic of photovoltaic material quality, and for thin films like CIGS, it has usually been measured by TRPL [4–8]. Two-photon excitation (2PE) TRPL measurements on thin polycrystalline samples can show similar values due to high surface and interface recombination; however, measurements on bulk wafers have shown lifetimes approaching 100 ns when carriers are generated more deeply in the bulk [9,10].

One-photon and 2PE TRPL measurements were collected using a mode-locked femtosecond laser with an optical parametric amplifier for tunable wavelength. A time-correlated single-photon counting system was used for these TRPL lifetime measurements. 2PE TRPL was applied to devices to provide the most uniform possible excitation of carriers throughout the device thickness. A wavelength of 1600 nm generated excess carriers, and a 1200 nm short-pass filter isolated the photoluminescence (PL) that was collected into the detector (an InGaAs single-photon counter). The excitation spot size was approximately 50–100 µm, which is large enough to neglect the effect of lateral diffusion of carriers from the original volume on the decay curve.

The 2PE-TRPL curves were collected as a function of forward bias applied to the CIGS cell. Even though 2PE was intended to excite carriers throughout the absorber layer thickness, the TRPL signal was still dominated by the carrier separation that is caused by the built-in field, where excess electrons and holes quickly moved in opposite directions and were no longer available for radiative recombination. TRPL decay times were short (in the ns range) for the open-circuited devices on all samples. Due to self-absorption, the collected PL signal mostly originated from near the junction surface [11].

The measurement of TRPL on a finished device is a function of charge separation and recombination. Forward bias was applied in an attempt to flatten the band potentials and isolate the carrier recombination. As a result, the decay times increased (up to tens of ns) with applied bias. A summary of decay times of all the samples is shown in Fig. 2. At high enough applied bias, forward current began to flow; to prevent significant device heating, voltage was limited to maintain a current within 2X to 3X of J_{SC}. Also, as forward bias was applied and excess carriers were injected across the junction, electroluminescence (EL) was generated. This EL emission occurred in the wavelength range

Download English Version:

https://daneshyari.com/en/article/6456629

Download Persian Version:

https://daneshyari.com/article/6456629

Daneshyari.com